Available online at www.sciencedirect.com
SCIENCE DIRECT®
Journal of the European Ceramic Society 25 (2005) 847–856
www.elsevier.com/locate/jeurceramsoc

Design and processing of Al_2O_3–Al_2TiO_5 layered structures

Salvador Bueno, Rodrigo Moreno, Carmen Baudín*

Instituto de Cerámica y Vidrio, CSIC, Campus de Cantoblanco, 28049 Madrid, Spain

Received 5 February 2004; received in revised form 22 April 2004; accepted 1 May 2004
Available online 10 July 2004

Abstract

Al_2O_3–Al_2TiO_5 layered composites were manufactured by a colloidal route from aqueous Al_2O_3 and TiO_2 suspensions with 50 vol.% solids. The mechanical behaviours of individual monolithic composite materials were combined and taken as basis for the design of the layered structures. Residual stresses which are likely to occur due to processing and thermally introduced misfits were calculated and considered for the manufacture of the laminates.

Monoliths with 10, 30 and 40 vol.% of second phase showed that increasing proportions of aluminium titanate decrease strength and increase the non-linear behaviour.

In order to obtain the desired combination of mechanical behaviours of the layers, two laminate designs with external and central layers of one composition and the alternating internal layer of the other composition were chosen taking into account chemical compatibility and development of residual stresses. In the system AA10, external and central layers of monophase Al_2O_3 with high strength were combined with intermediate layers of Al_2O_3 with 10 vol.% of Al_2TiO_5. The system A10A40 was selected to combine low strength and energy absorbing intermediate layers of Al_2O_3 with 40 vol.% of Al_2TiO_5 and sufficient strength provided by external layers of Al_2O_3 with 10 vol.% of Al_2TiO_5.

The stress–strain behaviour of the laminates was linear up to their failure stresses, with apparent strain for zero load after fracture larger than that corresponding to the monoliths of the same composition as that of the external layers. Moreover, the stress drop of the laminate samples occurred in step-like form thus suggesting the occurrence of additional energy consuming processes during fracture.

Keywords: Ceramic laminates; Slip casting; Sintering; Al_2O_3; Al_2TiO_5; Laminates

1. Introduction

Improved flaw tolerance and toughness with alumina (Al_2O_3)–aluminium titanate (Al_2TiO_5) composites have been reported previously.[1–6] The toughening mechanisms acting in these composites are crack bridging and microcracking and, therefore, toughening is often associated with rather low strength. Both mechanisms are originated by the residual stresses that develop during cooling from the sintering temperature due to thermal expansion mismatch between alumina and aluminium titanate.

In composite materials in which ceramic layers of different composition and, or microstructure are combined, the properties can be tailored to be superior to those of the constituent layers.[7] In particular, it is possible to achieve high flaw tolerance, without sacrificing strength, by using a laminate design in which an R-curve material is located between high strength layers, as demonstrated by Russo et al.[8] in the alumina–aluminium titanate system. These authors fabricated trilaminates with surface layers consisting of a homogeneous mixture of alumina–20 vol.% aluminium titanate and a flaw tolerant inner layer of the same composition with heterogeneous microstructure. As opposite to laminate design in which the high strength is due to residual compressive stresses acting in the outer layers,[9,10] such a design would assure also high strength for increasing temperature. The limit of this approach is the difficulty to obtain co-sintered layers of the same composition with large microstructural differences and, therefore, with significant differences in the mechanical behaviour.

In a previous work,[11] the processing conditions to achieve crack free and completely reacted alumina–aluminium titanate monolithic composites were established. Uniform distribution of the second phase was obtained by a strict control of the colloid chemistry of the mixture and grain growth was controlled by using a thermal treatment at relatively low temperature. Increased sintering temperature and aluminium titanate content led to microstructures with larger grains that presented non-linear stress–strain

* Corresponding author. Tel.: +34 91 735 5840; fax: +34 91 735 5843.
E-mail address: cbaudin@icv.csic.es (C. Baudín).

0955-2219/$ – see front matter © 2004 Elsevier Ltd. All rights reserved.
doi:10.1016/j.jeurceramsoc.2004.05.001

response,[12] in agreement with a simplified model[6,13] proposed for biphasic materials. Therefore, a combination of layers with different aluminium titanate contents might lead to simultaneous high strength and flaw tolerance, once the residual stresses due to the thermal expansion mismatch of layers with different composition are controlled.

In order to obtain the desired strength-flaw tolerance behaviour, the properties of the layer materials as well as the green processing and sintering conditions of the laminates need to be carefully adjusted. First, the composition and microstructure of the different layer materials should be optimised to achieve the suitable mechanical behaviour. Second, compatible processing conditions, in particular, sintering schedule, should be established to maintain the properties of the layers in the layered structure and impede the failure of the laminate during fabrication due to incompatible shrinkage of the layers. Last, residual stresses in the layers, originated by thermal expansion mismatch, have to be controlled to avoid fracture.

In this work, the processing parameters to obtain flaw tolerant and high strength laminates in the alumina–aluminium titanate system are investigated. Slip casting of aqueous alumina and titania mixtures with high solids contents allows to obtain composite materials with homogeneous microstructures and is a simple way to fabricate laminates constituted by relatively thick ($\cong$200–1000 μm) layers. Accurate control of the layer thickness can be reached by the control of the wall thickness formation rate and the sintering shrinkage of each slip formulation.

First, the influence of the volume fraction of aluminium titanate on the stress–strain response of the composites was studied, and from these results, characteristic layered structures with external layers of sufficient strength were designed. Second, the green processing and sintering conditions to fabricate laminates with controlled thickness of the different layers were selected on the basis of those for the monoliths, and recalculated with experimental results of sintered samples. Last, fracture of the laminates was characterised to check whether the desired mechanical behaviour was attained.

2. Experimental

The starting materials were commercial α-Al_2O_3 (Condea, HPA05, USA) and anatase-TiO_2 (Merck, 808, Germany) powders. Al_2O_3/TiO_2 mixtures with relative TiO_2 contents of 0, 5, 15 and 20 wt.% were prepared to obtain Al_2O_3/Al_2TiO_5 composites with Al_2TiO_5 concentrations of 0, 10, 30 and 40 vol.% after reaction sintering.

The single oxides and the mixtures were dispersed in deionised water by adding 0.5 wt.% (on a dry solids basis) of a carbonic acid based polyelectrolyte (Dolapix CE64, Zschimmer-Schwarz, Germany). Suspensions were prepared to a solids loading of 50 vol.% and ball milled with Al_2O_3 jar and balls during 4 h. These conditions were selected from a previous work.[11]

Rheological characterisation was carried out using a rotational rheometer (Haake, RS50, Germany) with a double cone/plate sensor system.

Solid discs with 20 mm in diameter were slip cast in plaster of Paris moulds in order to determine the casting rate of each suspension by measurement of the dry wall thickness (Mitutoyo, JDU25, Japan) after different casting times (1–16 min). For mechanical characterisation, plates with 70 mm × 70 mm × 10 mm dimensions were also obtained by slip casting for every composition. The cast bodies were carefully removed from the moulds and dried in air at room temperature for at least 24 h.

The reaction sintering behaviour of the specimens was studied with a differential dilatometer (Adamel Lhomargy, DI24, France) to 1550 °C. To obtain the monolithic materials, the dried blocks were sintered in air in an electrical box furnace (Termiber, Spain) at heating and cooling rates of 2 °C min^{-1}, with 4-h dwell at 1200 °C and 3-h dwell at the maximum temperature, 1550 °C.

The densities of the green and sintered compacts were determined by the Archimedes method using mercury and water, respectively. The crystalline phases present were determined by X-ray diffraction (Siemens AG, D5000, Germany) after grinding, and results were processed using the ASTM Files for corundum (42-1468), anatase (21-1272), rutile (21-1276) and β-aluminium titanate (26-0040).

The sintered blocks were machined into bars of 25 mm × 2 mm × 2.5 mm (referred to as small bars) for bend strength tests (three point bending, 20 mm span, 0.5 mm min^{-1}; Microtest, Spain) and dynamic Young's modulus (Grindosonic, Belgium). Nominal stress–apparent strain curves were calculated from the load values and the displacement of the central part of the samples recorded during the bend tests, and apparent Young's modulus was determined from the linear part of the curves. Reported bend strength and Young's modulus values are the average of five measurements and errors are the standard deviations.

To determine the thermal expansion curves of the monoliths, pieces of 10 mm × 5 mm × 5 mm were tested in a differential dilatometer (402 EP, Netzsch, Germany) using heating and cooling rates of 5 °C min^{-1}. From the recorded curves the average thermal expansion coefficients between 25 and 850 °C were calculated. Reported values are the average of three measurements and errors are the standard deviations.

Two layered composites of five layers were fabricated by alternately casting each suspension. Casting times were fixed to reach the desired layer thickness considering the casting kinetics and sintering shrinkage of each composition. One laminate, A10A40, had the central and outer layers ($\cong$1200 μm) made of A10(A+T) and the two inner layers ($\cong$300 μm) of A40(A+T). In the other system, AA10, the central and outer layers were made of alumina and the two inner layers of A10(A+T). Due to the geometry and dimen-

Table 1
Viscosity of suspensions and relative density (percent of theoretical) of monolithic samples

	Alumina	A10(A+T)	A30(A+T)	A40(A+T)
Viscosity (mPa s, 500 s^{-1})	34	43	44	51
ρ (green)	64.2 ± 0.5	63.9 ± 0.3	63.3 ± 0.5	62.5 ± 0.3
ρ (sintered)	98.2 ± 0.5	97.6 ± 0.4	97.8 ± 0.5	97.1 ± 0.4

sions of laminated architectures, bars of 25 mm × 5.5 mm × 3.5 mm for bend strength tests were obtained and tested under the same conditions as those described above. Bars of monolithic materials with the same dimensions than those of laminates were prepared for comparison. These are referred to as large bars.

Scanning electron microscopy (SEM, Carl Zeiss, DSM-950, Germany) was performed on the fracture surfaces and the width of the layers in the laminates was measured directly in the microscope. Additional SEM observations were performed on polished and chemically etched (HF 10 vol.%, 1 min) surfaces of the A10A40 laminates.

3. Results

3.1. Monoliths

The rheological properties of the studied suspensions were reported elsewhere.[11] All the suspensions used in this study

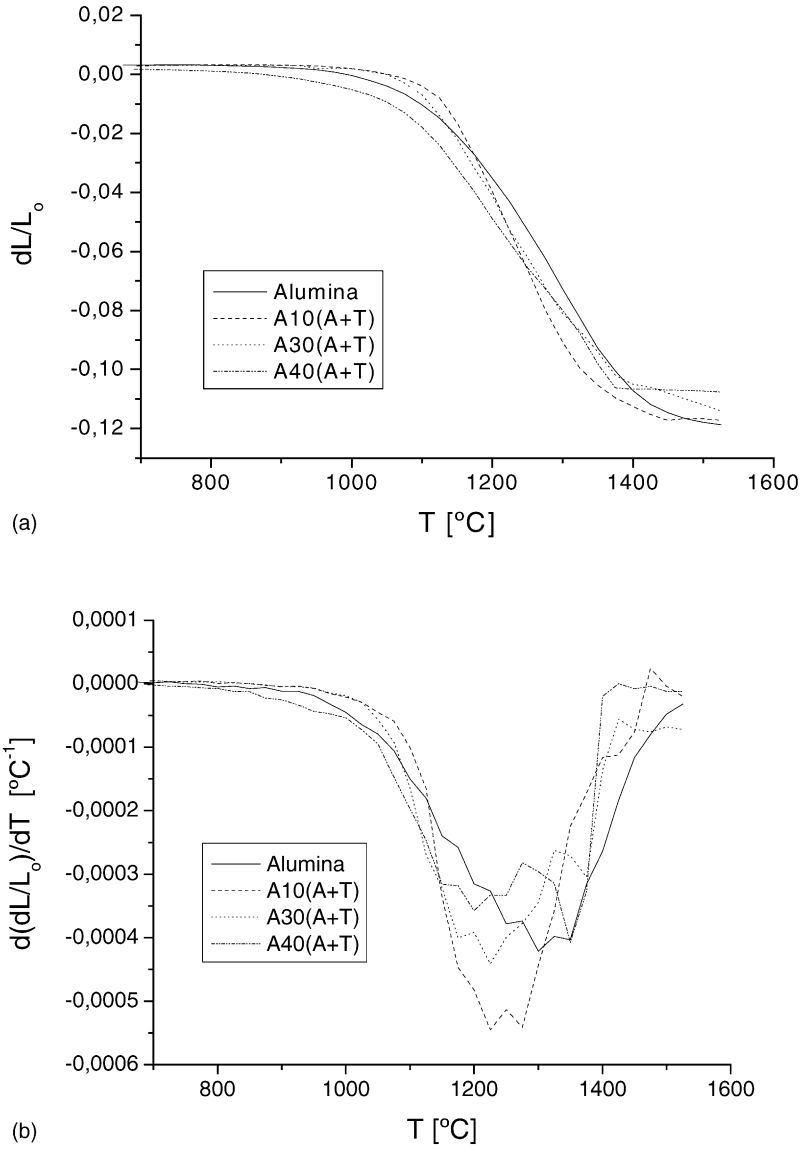

Fig. 1. Dynamic sintering curves of the monoliths. (a) Linear shrinkage, $\Delta L/L_0$, vs. temperature. (b) Linear shrinkage rate, $d(\Delta L/L_0)/dT$, vs. temperature.

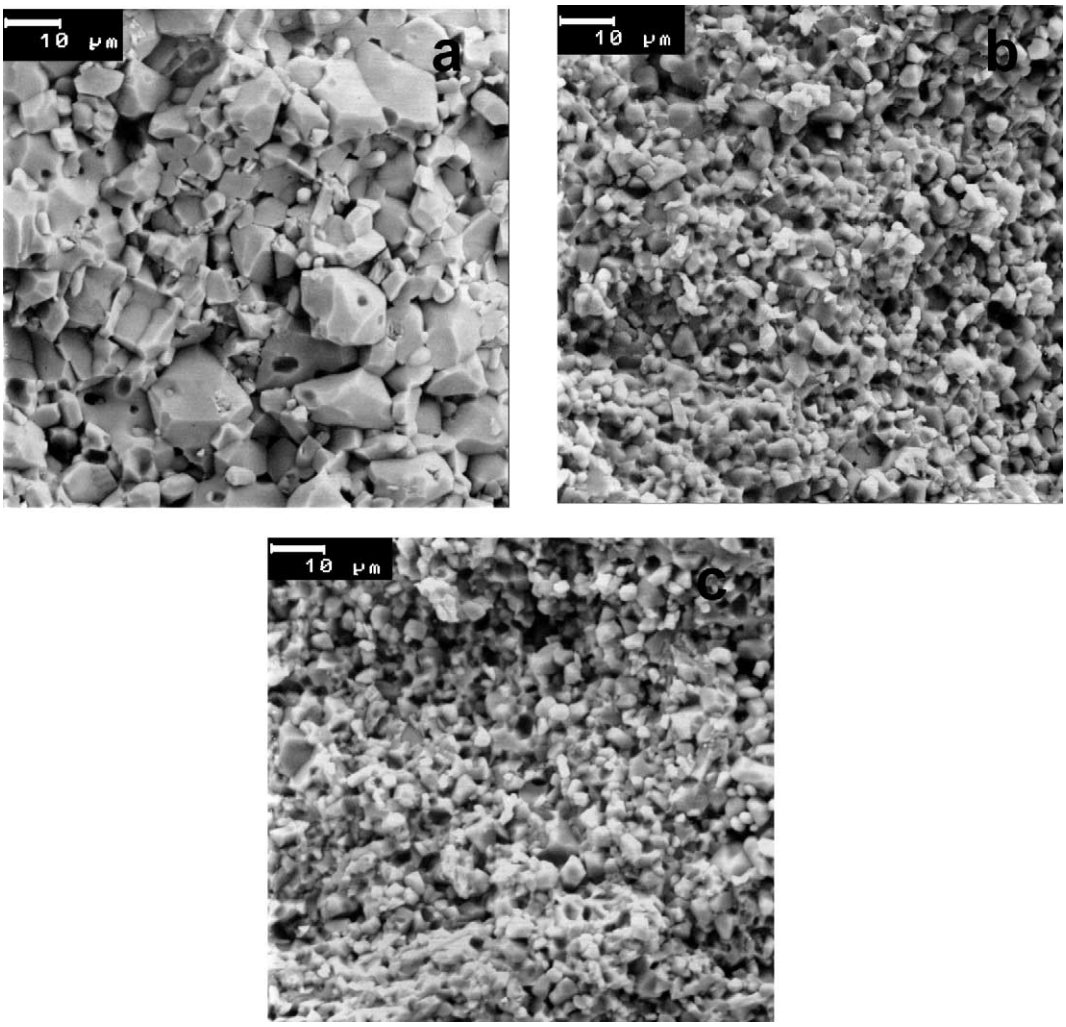

Fig. 2. Scanning electron micrographs of fracture surfaces of the monoliths (prepared with heating and cooling rates of 2 °C min^{-1}, with 4-h dwell at 1200 °C and 3-h dwell at the maximum temperature, 1550 °C). Alumina grains appear with dark grey colour, aluminium titanate of an intermediate grey shade and titania, which would appear white, is not observed. Tensile surfaces are located at the lower part of the micrographs. (a) A10(A+T); (b) A30(A+T); (c) A40(A+T).

had viscosities of ≈40–50 mPa s at a shear rate of 500 s^{-1} (Table 1). The optimised colloidal processing led to high green density composites (>62.5% of theoretical density, Table 1).

In Fig. 1, dynamic sintering curves for alumina and the three studied composites are plotted. For the composites, the shrinkage levels are coincident at 1240 °C (Fig. 1a) and the sintering rates are coincident at 1150 °C (Fig. 1b). These three curves exhibit a change of slope at temperatures of approximately 1380 °C.

In Fig. 2, characteristic fracture surfaces of the composite monoliths sintered at 1550 °C are observed. Aluminium titanate is homogeneously distributed and mainly located at alumina triple points and grain boundaries, and no titania is detected, according to XRD. In the samples with 10 vol.% of aluminium titanate (Fig. 2a) the grain size of alumina (≈5 μm) is much larger than in the samples containing 30 and 40 vol.% of aluminium titanate (Fig. 2b and c),

Characteristic nominal stress–apparent strain relations for the small (25 mm × 2 mm × 2.5 mm) monolithic samples are shown in Fig. 3a and the thermal expansion coefficient and mechanical properties are summarised in Table 2. The curves corresponding to the monolith with the lowest aluminium titanate content, A10(A+T), were practically linear up to fracture and this material presented the highest strength, Young's modulus and thermal expansion values and the lowest strains to fracture. Increasing proportions of aluminium titanate decrease strength, Young's modulus and thermal expansion and increase the non-linear behaviour, with high strains to fracture.

Fig. 4 shows characteristic fracture surfaces of the three monoliths at low magnification. Those of A10(A+T)

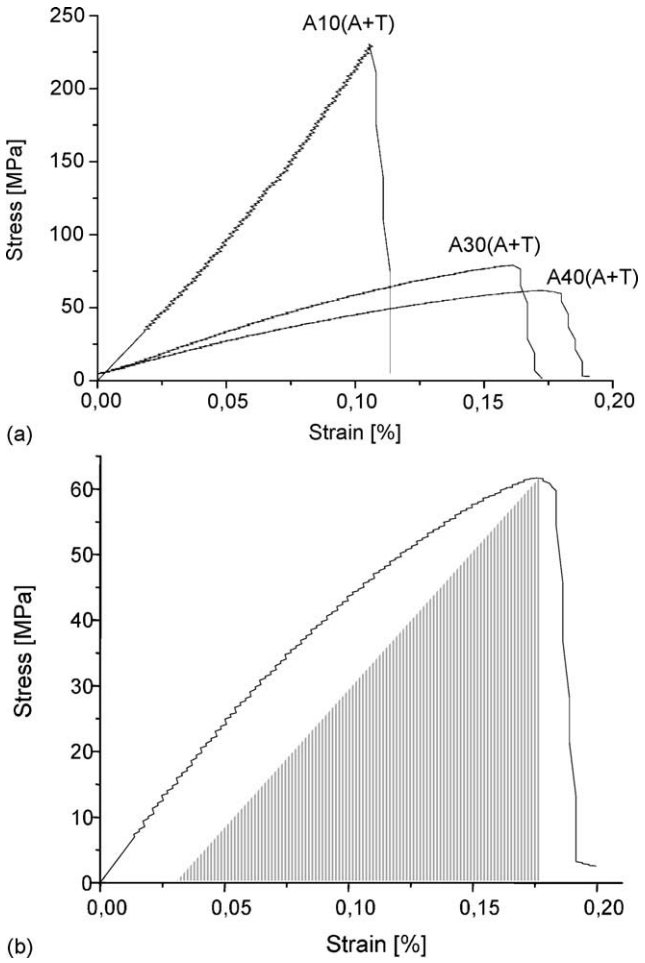

Fig. 3. Characteristic nominal stress–apparent strain curves for monolithic small (25 mm × 2 mm × 2.5 mm) samples. (a) Curves corresponding to the materials indicated. (b) Characteristic ratio of specific elastic energy at fracture (scratched area) to the whole specific energy expended during the test for A40(A+T) materials.

samples were flat whereas those of the A30(A+T) and A40(A+T) samples were highly tortuous.

3.2. Laminates

Two laminates with five layers were fabricated. The system A10A40 combines intermediate layers of A40(A+T) composition with central and external layers of A10(A+T) composition. In the system AA10, external and central layers of monophase alumina were combined with intermediate layers of A10(A+T) composition. As discussed below, thin intermediate layers (≈300 μm) and thick external and central layers (≈1200 μm) were selected.

Fig. 5 shows the casting kinetics for the alumina and the three composite slips. In all cases, the well-known proportionality between wall thickness (l) and the square root of time (t) is found.[14] Casting time shortens with titania content for the same wall thickness.

Fig. 6 shows characteristic fracture surfaces of the layered materials where the different layers are easily differentiated because the crack path changes at the interlayers. Nevertheless, the size of the layers indicated in Table 3, which was measured directly in the SEM on fracture surfaces, has to be taken as approximate.

In Fig. 7, the nominal stress–apparent strain relationships of the laminates are compared to those for large monolithic samples (25 mm × 5.5 mm × 3.5 mm) with the same compositions as those of the corresponding external layers. In all cases, the behaviour was practically linear up to fracture. The slope of the linear portion was lower for the layered materials. The stress drop from the failure point occurred steeply for the monoliths, in which apparent deformation at the maximum load was coincident with that for zero load after fracture. In the laminates, a step-like way was followed and apparent strain for zero load was larger than that corresponding to failure load.

Strength values for the laminates were 272 ± 32 MPa and 147 ± 20 MPa, for AA10 and A10A40, respectively.

4. Discussion

4.1. Monoliths

The objective of this work was the development of laminates on the basis of the properties of the monolithic composite materials that would constitute the different layers. Therefore, the selection of the sintering schedule for the monoliths was performed to ensure the possibility of laminate fabrication. Moreover, complete reaction between

Table 2
Thermal expansion coefficient and mechanical properties of monolithic materials

	Alumina	A10(A+T)	A30(A+T)	A40(A+T)
$\alpha_{25–850\,^{\circ}C}$ × 10^{-6} ($^{\circ}C^{-1}$)	8.8 ± 0.2	8.3 ± 0.3	4.7 ± 0.2	4.1 ± 0.1
$E_{dynamic}$ (GPa)	388 ± 5	333 ± 9	146 ± 6	107 ± 3
E_{static} (GPa)	376 ± 6	202 ± 10	60 ± 8	43 ± 1
Brittleness parameter	–	0.99 ± 0.01	0.76 ± 0.03	0.72 ± 0.03
Bending strength (MPa)				
Small samples (25 × 2 × 2.5)	–	230 ± 1	76 ± 4	61 ± 1
Large samples (25 × 5.5 × 3.5)	304 ± 36	189 ± 6	62 ± 2	43 ± 1

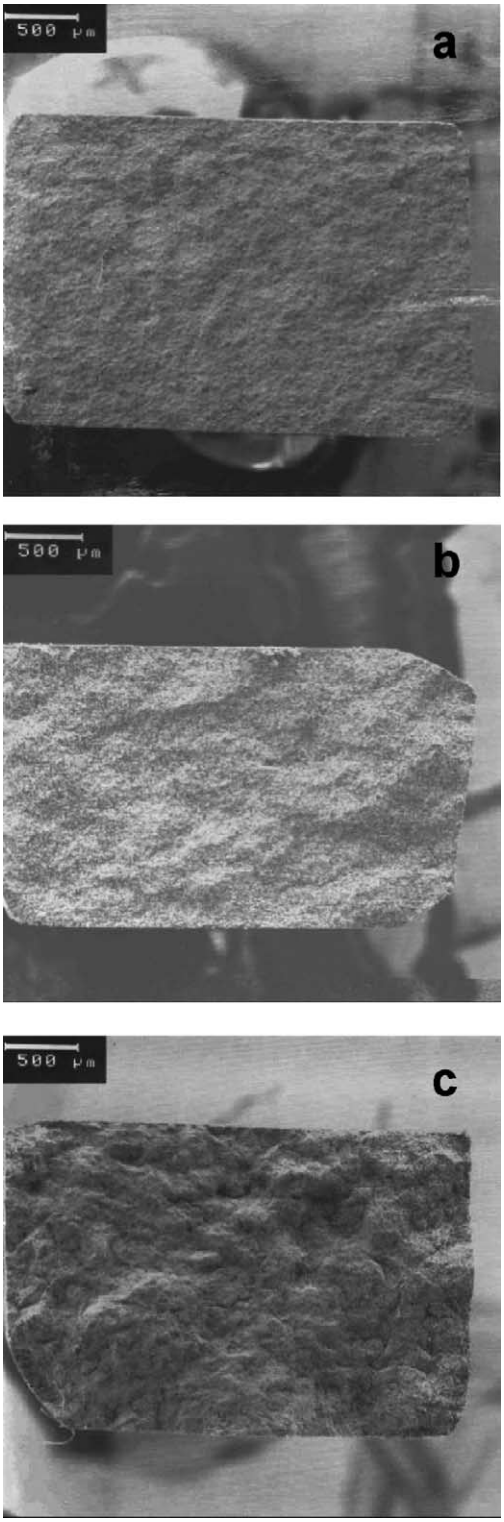

Fig. 4. Low magnification scanning electron micrographs of fracture surfaces of monolith samples (25 mm × 2 mm × 2.5 mm). The tensile surfaces are located at the lower part of the micrographs. (a) A10(A+T); (b) A30(A+T); (c) A40(A+T).

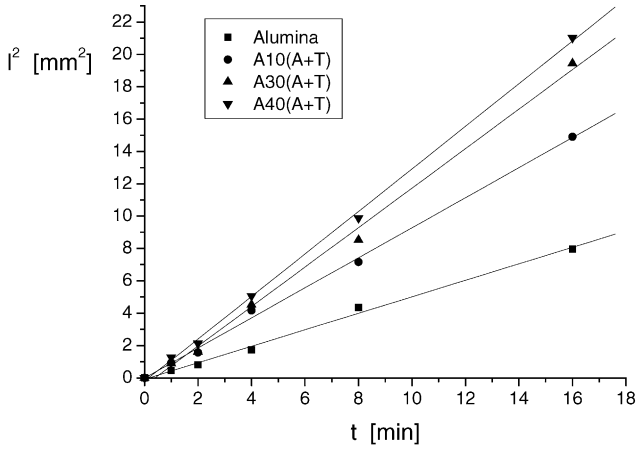

Fig. 5. Square wall thickness, l^2, vs. casting time for alumina and alumina–titania aqueous suspensions.

Al_2O_3 and TiO_2 to form Al_2TiO_5 and sufficient grain growth as to originate microcracking and, consequently, non-linear stress–strain behaviour in the compositions with high Al_2TiO_5 contents were also to be achieved. To satisfy these two latter requirements rather high final sintering temperatures (>1450 °C)[11,12] whereas are needed, in order to allow co-sintering of the different compositions in the laminates, similar shrinkage levels as well as shrinkage rates through the temperature range are preferred.

In Fig. 1, the change of slope in the dynamic sintering curves for the composites at approximately 1380 °C is in agreement with the reported temperature for the expansive reaction between Al_2O_3 and TiO_2 to form aluminium titanate.[15] From these curves, a two-step sintering treatment, with a rather low heating rate 2 °C min^{-1}, was designed. An initial dwell of 4 h at 1200 °C was chosen for homogeneous shrinkage before reaction, this temperature being a compromise between those for coincident levels of shrinkage, 1240 °C, and of shrinkage rate, 1150 °C. In this temperature range, the alumina compacts have similar levels of shrinkage and shrinkage rate as those of the composite with the lowest titania contents. A 3-h dwell at 1550 °C was selected for final reaction and grain growth, as this was the temperature at which shrinkage was arrested in the three composites.

Using this sintering schedule, dense (Table 1) and reacted, at least at the XRD level, materials were obtained. The second phase, Al_2TiO_5, was homogeneously distributed as small particles located mostly at triple points of the alumina matrix (Fig. 2).

As shown in Fig. 2, extreme differences are found between grain sizes of alumina in the A10(A+T) composite and in those containing larger quantities of aluminium titanate, which are much smaller. This is due to the inhibiting effect of the second phase in matrix grain growth, and indicate that most alumina grain growth occurs after the formation of aluminium titanate.

Compositional differences originate highly different thermal expansion values and deformation and fracture

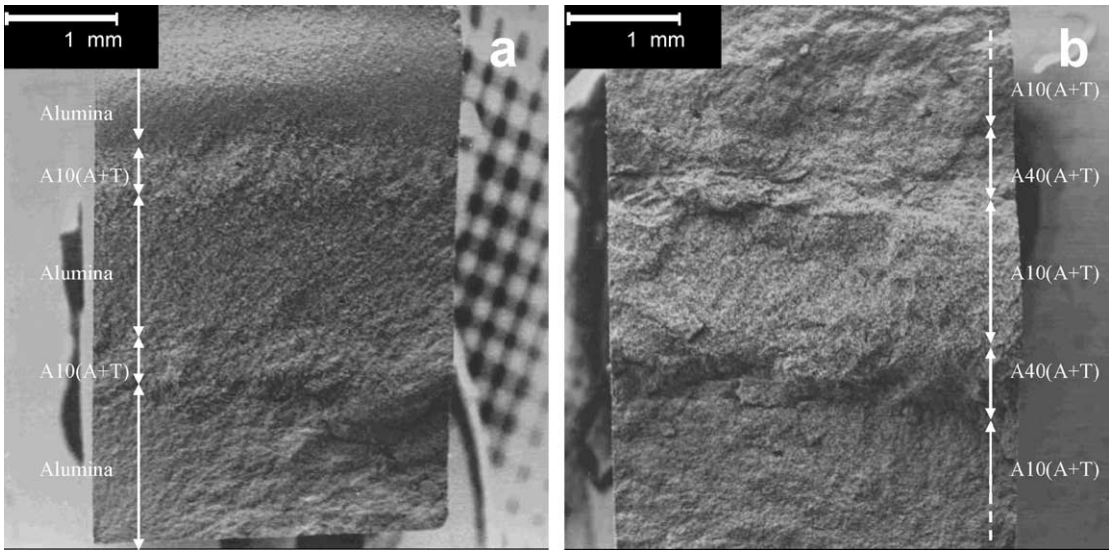

Fig. 6. Scanning electron micrographs of characteristic fracture surfaces of the laminates. The tensile surfaces are located at the lower part of the micrographs. (a) AA10; (b) A10A40.

behaviours of the composites due to the occurrence of microcracking at different levels, as discussed below.

Thermal expansion and dynamic Young's modulus are the highest for alumina and the composite containing the lowest amount of aluminium titanate (Table 2). For alumina, these values are in the range of those of dense and fine grained uncracked materials, and they are slightly lower in the 10(A+T) composite which, in principle, might be attributed to the presence of Al_2TiO_5. In this way, the material A10(A+T) presented linear behaviour up to fracture, similar to monophase alumina, steeply stress drop and the lowest strains at fracture, as compared with the composites with higher Al_2TiO_5 contents (Fig. 3a), in agreement with the smooth fracture surfaces of these samples (Fig. 4a). This fracture behaviour is characteristic of non-microcracked materials. There are differences between alumina and 10(A+T)

Table 3
Casting time and comparison between the obtained and calculated thickness for the layers

	Casting time (s)	Calculated thickness (μm)	Obtained thickness (μm)
A10A40			
A10(A+T)—Layer 1	313	2200	–
A40(A+T)—Layer 2	70	300	360–390
A10(A+T)—Layer 3	481	1200	1200–1240
A40(A+T)—Layer 4	115	300	390–420
A10(A+T)—Layer 5	1449	2200	–
AA10			
Alumina—Layer 1	639	2200	–
A10(A+T)—Layer 2	91	300	300–330
Alumina—Layer 3	996	1200	1400–1500
A10(A+T)—Layer 4	149	300	310–335
Alumina—Layer 5	3005	2200	–

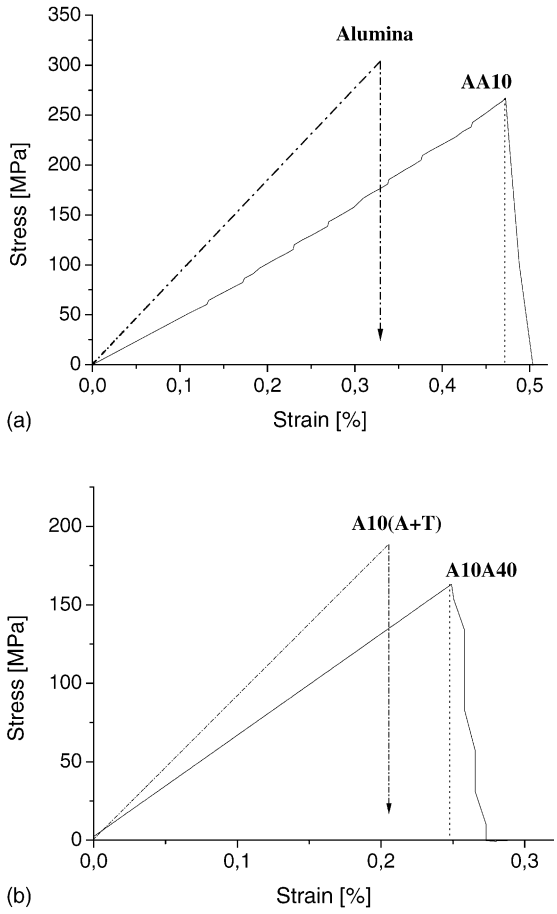

Fig. 7. Characteristic nominal stress–apparent strain curves for laminates compared to those for thick (25 mm × 5.5 mm × 3.5 mm) monolith samples with the same compositions as those of the corresponding external layers. (a) AA10 and alumina; (b) A10A40 and A10(A+T).

when static Young's modulus is considered, as it is much lower for the composite and significantly different from dynamic Young's modulus (Table 2). The former parameter is more sensible to microcracks because of the larger deformations imposed during the tests as compared to those imposed in dynamic measurements. Accordingly, the fact that the static Young's modulus for A10(A+T) is significantly lower than the dynamic modulus would indicate that deformation imposed during loading originates incipient microcracking in the material, undetectable by a changing of the curvature of the nominal stress–apparent strain curve (Fig. 3a).

In the materials A30(A+T) and A40(A+T) the lower strength values (Table 2), large strains at fracture and non-linear behaviour are due to the presence of microcracks, which originate highly tortuous fracture (Fig. 4b and c) revealing additional energy absorption during the fracture process. These microcracks lead to low values of the dynamic and static Young's modulus and thermal expansion (Table 2).

In order to select the most adequate material to constitute the internal flaw tolerant layers in the laminates, the brittleness parameter proposed by Gogotsi[16] can be used to quantify the apparent ductility of the two composites containing the largest aluminium titanate amounts. This parameter is defined by the ratio of the specific elastic energy which has been accumulated in the sample at fracture, calculated from the apparent Young's modulus and the elastic deformation at fracture, to the whole specific energy expended during the test, determined as the whole area under the stress–strain curve (Fig. 3b). As shown in Table 2, the brittleness parameter is the lowest, indicating larger apparent ductility, for the composite containing 40 vol.% of aluminium titanate. This apparent ductility leads to increased energy absorption during fracture in the expense of strength, as demonstrated by the fact that only one-fourth of the strength of the A10(A+T) monolith is achieved by these samples.

4.2. Laminates

From the above-mentioned results, two laminates with five layers were designed. The system A10A40 was selected to combine low strength and energy absorbing intermediate layers of A40(A+T) composition with sufficient strength provided by external layers of A10(A+T) composition, which was preferred over monophase alumina because of chemical compatibility between the layers. In the system AA10, external and central layers of monophase alumina with high strength were combined with intermediate layers of A10(A+T) composition, in which microcracks might be developed at most during loading, as discussed above. For symmetry, both laminates were designed with internal central layers of the same composition as that of the corresponding external layer.

Considering Young's modulus and thermal expansion coefficients values, given in Table 2, tensile residual stresses are expected in the external and central A10(A+T) and alumina layers in the laminates A10A40 and AA10, respectively. Since residual stresses reduce the strength, thin ($\sim$300 μm) intermediate layers and relatively thick ($\sim$1200 μm) external and central layers were selected to minimise them. With such structure, negligible residual stresses would be developed in the system AA10 in which high strength values are expected.

For the preparation of laminates, suspensions with low viscosity and high solids content result in a better control of wall thickness formation. Casting rates of 0.53 and 1.31 $mm^2\,min^{-1}$ (corresponding to the slopes of the kinetics curves in Fig. 5) are found for alumina and A40(A+T), respectively, which allow a good control of the casting process. The layered green bodies were fabricated by sequential slip casting. The thickness of each layer in the laminates was controlled by recalculating the casting time taking into account the sintering shrinkage experienced by the monoliths with the same compositions as those of the layers. Table 3 summarises casting times and the comparison between the obtained thickness of the layers, measured directly in the SEM, and the calculated ones. There are significant differences ($\approx$25–35%) between the calculated and the obtained widths for the layers made from the A40(A+T) slips, whereas those corresponding to the A10(A+T) slips are inside the uncertainty range associated with the measurement method and the variability between samples. This fact is explained in terms of slip quality, as the one made of A40(A+T) mixture presented the poorest rheological behaviour, thus making the control of casting rate difficult. For the alumina layers, very high casting times ($\approx$1000 s for the central layer, Table 3) are necessary and therefore a possible change in the slip properties could modify the casting kinetics and the obtained thickness.

A comparison between the stress–strain behaviour of the sintered laminates and that of monolith samples of the same size is established in Fig. 7. The stress–strain behaviour of the laminate A10A40 was linear up to fracture, such as that of the monoliths that constituted its external and central layers, made of 10(A+T). This fact indicates that the external and central uncracked layers dominate this deformation range. The monolith AA10 behaves also linearly, as both constituents. Nevertheless, the slope of this linear portion was lower for the layered materials than for the large monolithic samples with the same composition as those of the corresponding external layers, due to the effect of the low Young's modulus internal layers.

The stress drop from the failure point of the large monolith samples occurred steeply, and apparent deformation at the maximum load was coincident with that for zero load after fracture (Fig. 7). In the laminates, a step-like way was followed and apparent strain for zero load was larger than that corresponding to failure load. This fracture behaviour is related to the changes in the crack path at the interlayers, as suggested by the fracture surfaces (Fig. 6). The effect is more significant for A10A40 (Fig. 7b) in which, in addition to the crack deflection due to differences between

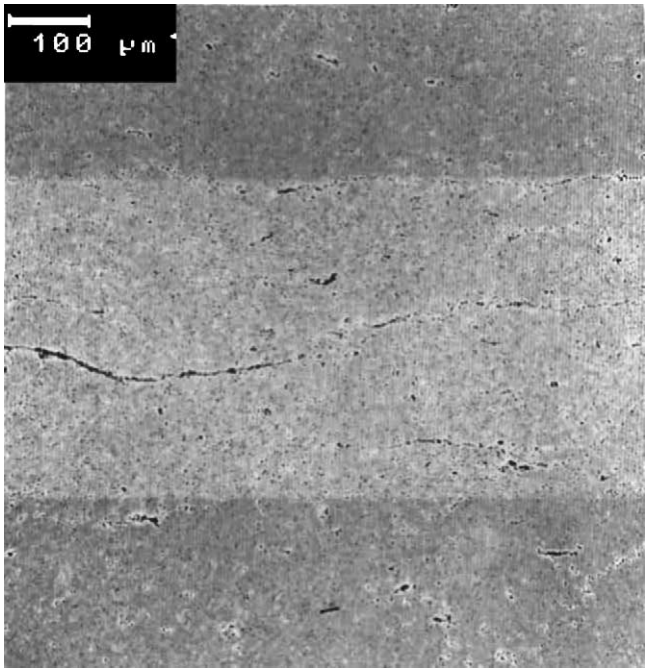

Fig. 8. Scanning electron micrographs of characteristic edge crack observed in A40(A+T) layer of polished and chemically etched (HF 10%, 1 min) surface in the A10A40 material.

the fracture behaviour of the different layers, as focused by the material design, crack bifurcation due to compression in the internal A40(A+T) layers may also occur. The presence of these compressive stresses is demonstrated by the occurrence of edge cracks[17] as those shown in Fig. 8. Both, crack deflection and crack bifurcation imply the occurrence of additional energy consuming processes during fracture in the laminates.

The fact that strength values for the system A10A40 (147 ± 20 MPa) were lower (∼25%) than those of the monolith with the same composition as that of the external layer, A10(A+T), can be attributed to the residual stresses developed in the external layer during cooling from the sintering temperature. Calculations[18] show that, in the laminate A10A40, compressive stresses of ≈500 MPa and tensile stresses of ≈90 MPa would develop in the A40(A+T) and A10(A+T) layers, respectively, and, therefore, a strength decrease of up to 40% could be expected for the A10(A+T) layer in the laminate. As discussed above, residual stresses are not significant in AA10 and, consequently, strength values in this system are of the same order as those for alumina monoliths.

From the above discussion it is clear that different behaviours can be achieved by combination of composite layers in the system Al_2O_3–Al_2TiO_5. Further studies will be dedicated to establish the effect of different stacking orders and layer thickness on the mechanical behaviour of the laminates. Moreover, detailed fracture studies in terms of crack propagation will help to understand the fracture behaviour of the laminates.

5. Conclusions

The fracture behaviour of monolithic Al_2O_3–Al_2TiO_5 materials with 0, 10, 30, and 40 vol.% second phase was studied, showing that increasing proportions of aluminium titanate decrease strength and increase the non-linear behaviour.

The studied system is adequate to obtain layered composites with very different mechanical behaviours, selected as a function of the behaviour of the constituent Al_2O_3–Al_2TiO_5 layers and their thermal expansion mismatch.

In particular, two laminate designs were fabricated to combine the desired properties of external layers with linear stress–strain behaviour up to fracture and relatively high strength, with larger strains to fracture provided by the internal layers. One of them presented fracture strength values lower than those of alumina and significant step-like fracture. The second presented strength values close to those of alumina and step-like fracture in a lesser extent.

Acknowledgements

Work supported in part by the European Community's Human Potential Programme under contract HPRN-CT-2002-00203, [SICMAC], by the project MAT2003-00836 and by the grant CSIC I3P-BPD2001-1 (Spain).

References

1. Runyan, J. L. and Bennison, S. J., Fabrication of flaw-tolerant aluminum-titanate-reinforced alumina. *J. Eur. Ceram. Soc.* 1991, **7**, 93–99.
2. Padture, N. P., Bennison, S. J. and Chan, H. M., Flaw-tolerance and crack-resistance properties of alumina–aluminium titanate composites with tailored microstructures. *J. Am. Ceram. Soc.* 1993, **76**, 2312–2320.
3. Bartolomé, J., Requena, J., Moya, J. S., Li, M. and Guiu, F., Cyclic fatigue crack growth resistance of Al_2O_3–Al_2TiO_5 composites. *Acta Mater.* 1996, **44**, 1361–1370.
4. Bartolomé, J., Requena, J., Moya, J. S., Li, M. and Guiu, F., Cyclic fatigue of Al_2O_3–Al_2TiO_5 composites in direct push-pull. *Fatigue Fract. Eng. Mater. Struct.* 1997, **20**, 789–798.
5. Uribe, R. and Baudín, C., Influence of a dispersion of aluminum titanate particles of controlled size on the thermal shock resistance of alumina. *J. Am. Ceram. Soc.* 2003, **86**, 846–850.
6. Padture, N. P., Runyan, J. L., Bennison, S. J., Braun, L. M. and Lawn, B. R., Model for toughness curves in two-phase ceramics: II. Microstructural variables. *J. Am. Ceram. Soc.* 1993, **76**, 2241–2247.
7. Chan, H. M., Layered ceramics: processing and mechanical behaviour. *Annu. Rev. Mater. Sci.* 1997, **27**, 249–282.
8. Russo, C. J., Harmer, M. P., Chan, H. M. and Miller, G. A., Design of a laminated ceramic composite for improved strength and toughness. *J. Am. Ceram. Soc.* 1992, **75**, 3396–4000.
9. Lakshminarayanan, R., Shetty, D. K. and Cutler, R. A., Toughening of layered ceramics composites with residual surface compression. *J. Am. Ceram. Soc.* 1996, **79**, 79–87.
10. Wang, H. and Hu, X., Surface properties of ceramic laminates fabricated by die pressing. *J. Am. Ceram. Soc.* 1996, **79**, 553–556.

11. Bueno, S., Moreno, R. and Baudín, C., Reaction sintered Al_2O_3/Al_2TiO_5 microcrack-free composites obtained by colloidal filtration. *J. Eur. Ceram. Soc.*, in press.
12. Bueno, S., Moreno, R. and Baudín, C., Colloidal Processing of laminates in the system alumina-titania. *Key Eng. Mater.*, in press.
13. Lawn, B. R., Padture, N. P., Braun, L. M. and Bennison, S. J., Model for toughness curves in two-phase ceramics: I. Basic fracture mechanics. *J. Am. Ceram. Soc.* 1993, **76**, 2235–2240.
14. Tiller, T. M. and Tsai, C., Theory of filtration of ceramics: I. Slip casting. *J. Am. Ceram. Soc.* 1986, **69**, 882–887.
15. Freudenberg, B. and Mocellin, A., Aluminium titanate formation by solid-state reaction of fine Al_2O_3 and TiO_2 powders. *J. Am. Ceram. Soc.* 1987, **70**, 33–38.
16. Gogotsi, C. A., The use of brittleness measure (χ) to represent mechanical behaviour of ceramics. *Ceram. Int.* 1989, **15**, 127–129.
17. Ho, S., Hillman, C., Lange, F. F. and Suo, Z., Surface cracking in layers under biaxial, residual compressive stress. *J. Am. Ceram. Soc.* 1995, **78**, 2353–2359.
18. Virkar, A. V., Huang, J. L. and Cutler, R. A., Strengthening of oxide ceramics by transformation-induced stresses. *J. Am. Ceram. Soc.* 1987, **70**, 164–170.